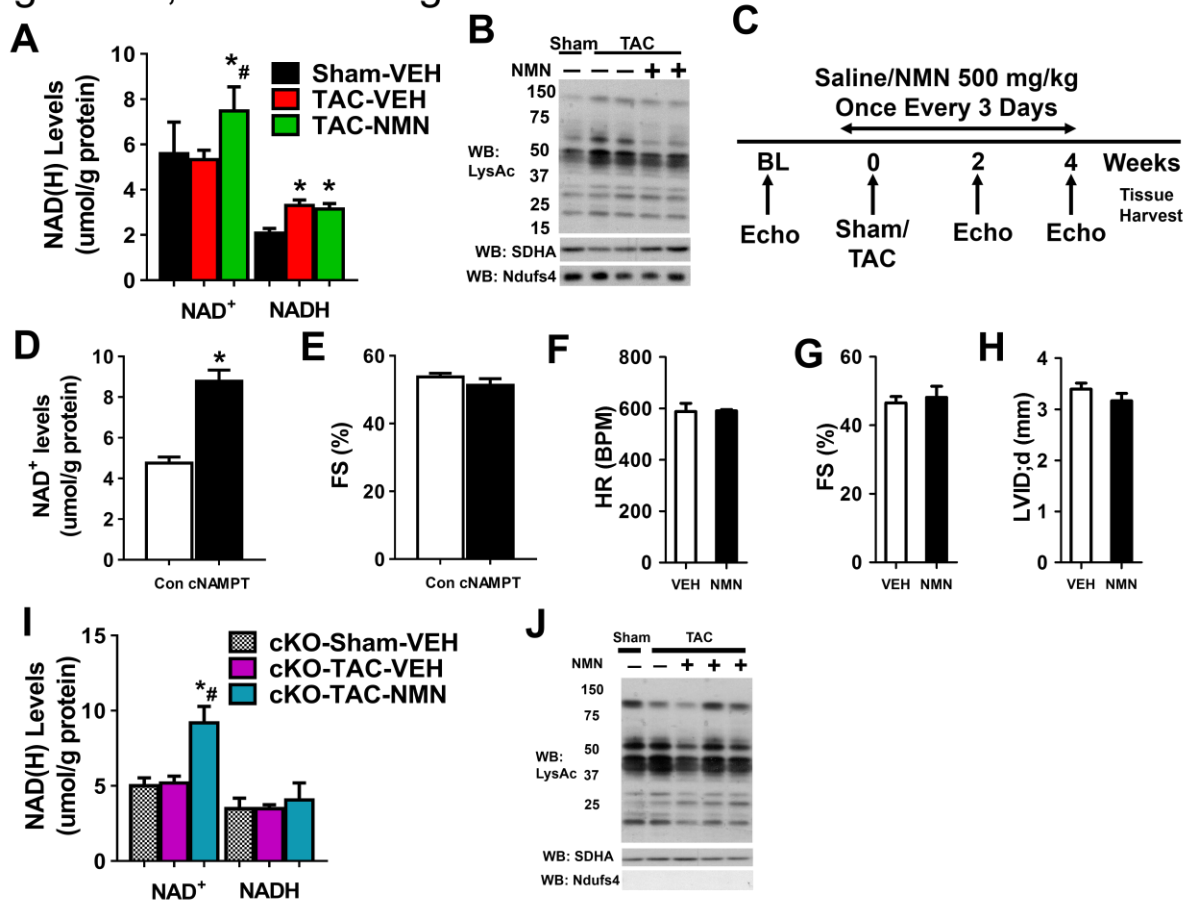


Supplementary material

Supplemental figure and figure legends

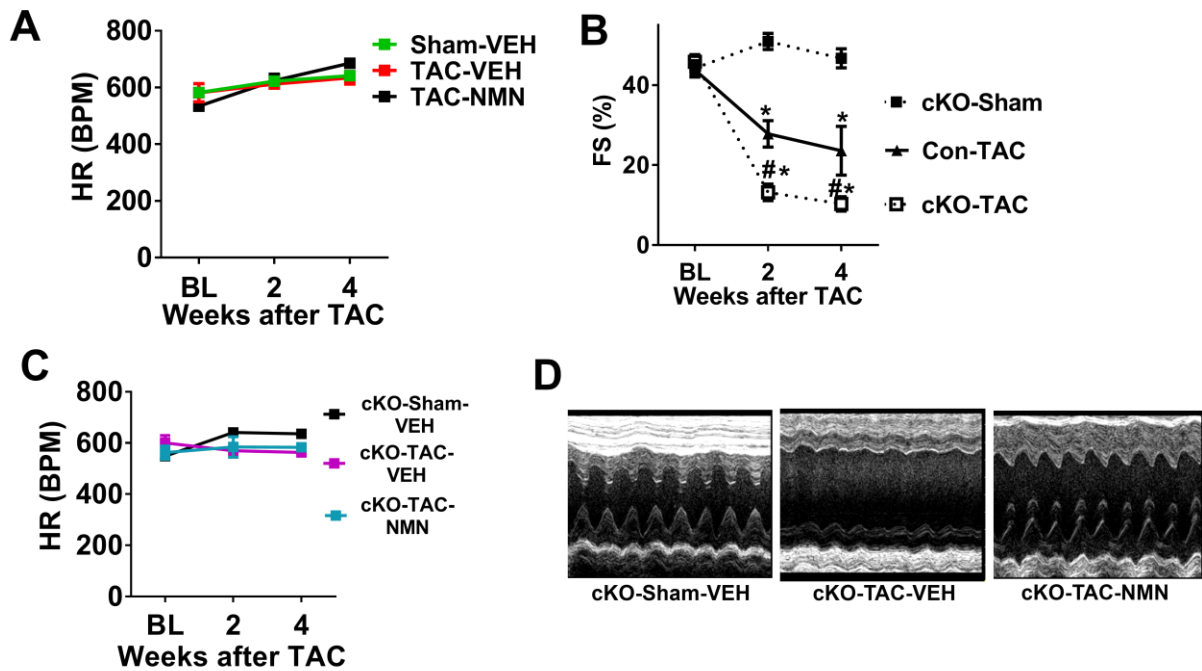
Figure S1, related to Fig 1



**Figure S1. Effects of elevation of cardiac NAD<sup>+</sup> levels by NMN administration on acetylation and cardiac function. (A)** NAD(H) levels from mitochondria of control mice after sham or TAC surgeries with and without NMN treatment were measured. \*: P<0.05 compared to Sham-VEH. #: P<0.05 compared to TAC-VEH. **(B)** Representative Western Blotting of acetylation of mitochondria isolated as indicated. **(C)** Experimental plan for sham/TAC surgeries, treatments, and echocardiography (echo). **(D)** NAD<sup>+</sup> levels and **(E)** fractional shortening (FS) of control and cNAMPT hearts were measured. **(F)** Heart rate (HR), **(G)** FS, **(H)** left ventricle LVID:d (mm), **(I)** NAD(H) levels from mitochondria of control mice after sham or TAC surgeries with and without NMN treatment were measured. \*: P<0.05 compared to Sham-VEH. #: P<0.05 compared to TAC-VEH. **(J)** Representative Western Blotting of acetylation of mitochondria isolated as indicated. N=3. \*: P<0.05 compared to Control.

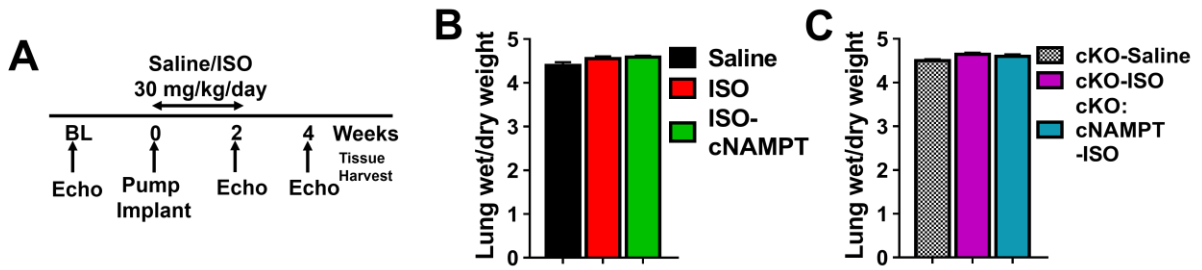
internal dimension at diastole (LVID;d) of vehicle (VEH, saline) or NMN (500 mg/kg) treated cKO mice were measured. N=3. NAD(H) levels of cKO hearts after sham or TAC surgeries and NMN treatment were measured. **(I)** NAD(H) levels of cKO hearts after sham or TAC surgeries and NMN treatment were measured. **(J)** Representative Western Blots measuring acetylation, SDHA and Ndufs4 levels of mitochondria isolated as indicated. N=3-4. \*: P<0.05 compared to corresponding Sham; #: P<0.05 compared to corresponding TAC. Data are expressed as means  $\pm$ SEM.

Figure S2 related to Fig 2



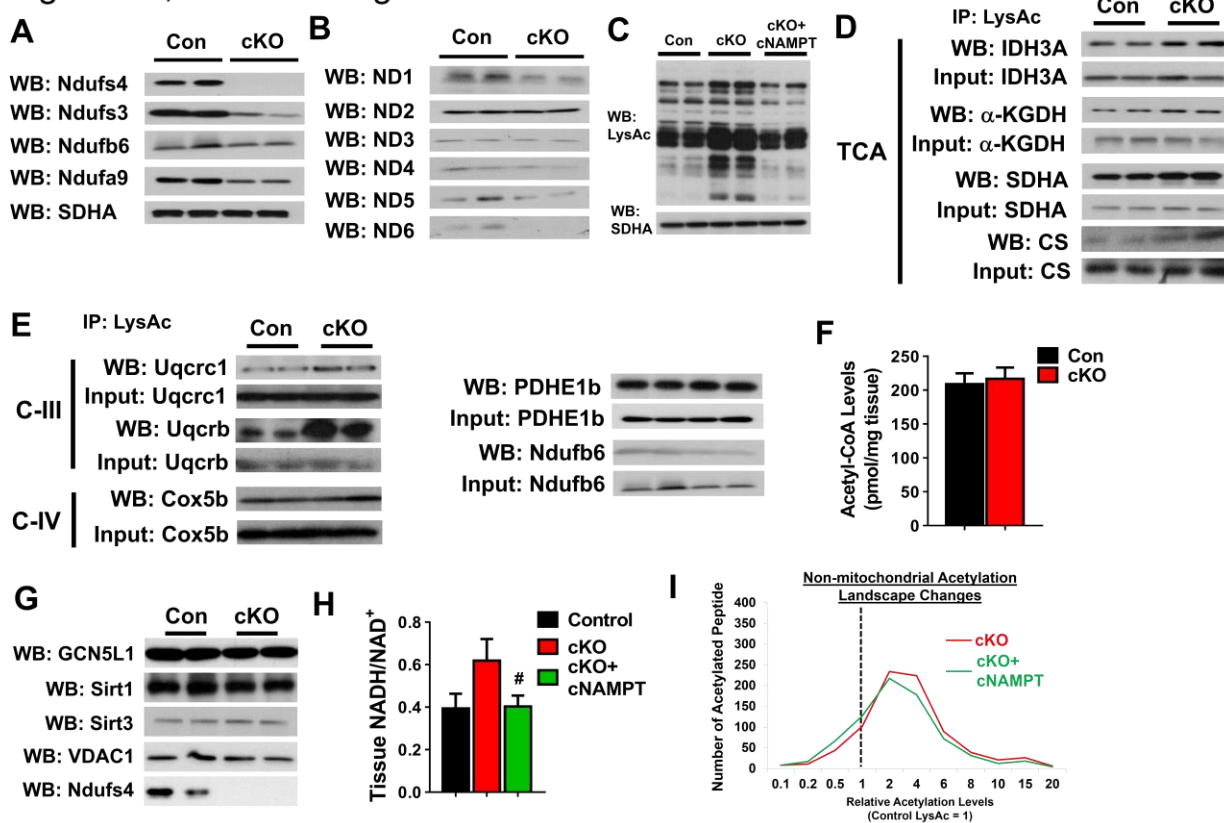
**Figure S2. Effects of NMN treatment on cardiac function after TAC. (A)** Heart rate (HR) of control mice after sham or TAC surgeries with and without NMN treatment were recorded. N=4-8. **(B)** FS of control and cKO mice after Sham/TAC surgeries at baseline (BL), 2 and 4 weeks after TAC. N=5-8. \*: P<0.05 compared to cKO-Sham; #: P<0.05 compared to Con-TAC. **(C)** HR of cKO mice treated as indicated were assessed. N=5-6. **(D)** Representative M-mode images from mice indicated. Data are expressed as means  $\pm$ SEM.

Figure S3, related to Fig 3



**Figure S3. Effect of cNAMPT expression on lung edema of mice after isoproterenol stimulation. (A)** Experimental plan for saline/ISO treatment and echocardiography (echo). **(B-C)** The ratio of wet/dry lung weight of indicated mice were measured. N=5-9. Data are expressed as means  $\pm$ SEM.

Figure S4, related to Fig. 4



**Figure S4. Complex I proteins, acetylation of mitochondrial proteins, acetyl-coA, Sirtuins and GCN5L1 levels in cKO and effects of cNAMPT on acetylation landscape.** Representative Western blots of C-I proteins contributed from **(A)** nuclear and **(B)** mitochondrial genomes from control and cKO mitochondrial lysates. N=4. **(C)** Representative Western blot for ac levels of indicated hearts. Acetylation levels of **(D)** TCA, **(E)** ETC proteins, PDHE1b and Ndufs6 were assessed by immunoprecipitation/Western blot (IP-WB) analysis. N=4. **(F)** Acetyl-coA levels of cardiac tissues as indicated were measured. N=4. **(G)** Protein levels of mitochondrial acetyltransferase GCN5L1, and deacetylases Sirt1/3, in control or cKO mitochondria were measured. VDAC and Ndufs4 as controls. **(H)** Tissue NADH/NAD<sup>+</sup> ratio of indicated hearts were measured and **(I)** Non-mitochondrial acetylation landscape

changes of cKO and cKO+cNAMPT hearts were compared. N=4. #: P<0.05 compared to cKO. Data are expressed as means  $\pm$ SEM.

Figure S5, related to Fig. 5

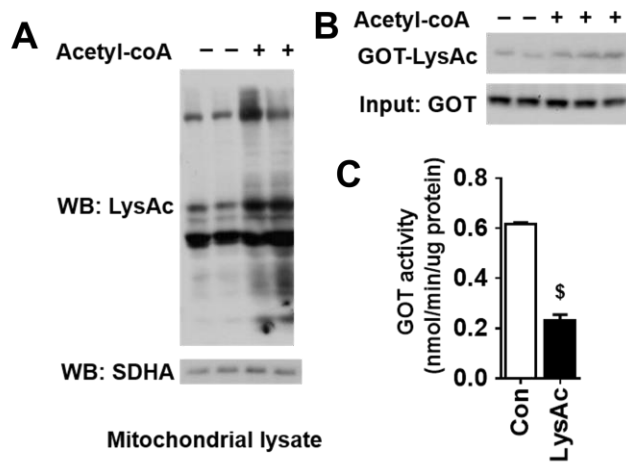


**Figure S5. In vitro acetylation of mitochondrial proteins by acetyl-coA. (A)**

Mitochondrial lysates were incubated with or without acetyl-coA (1.5 mM) for six hours and acetylation levels were probed with anti-acetyl-lysine antibody. **(B)** The acetyl-coA-treated mitochondrial lysates were immunoprecipitated with anti-acetyl-lysine antibody coupled agarose and probed for the presence of GOT2 protein. **(C)** The GOT activities of the non-acetylated and acetylated lysates were measured.

## Figure S6, related to Fig. 6

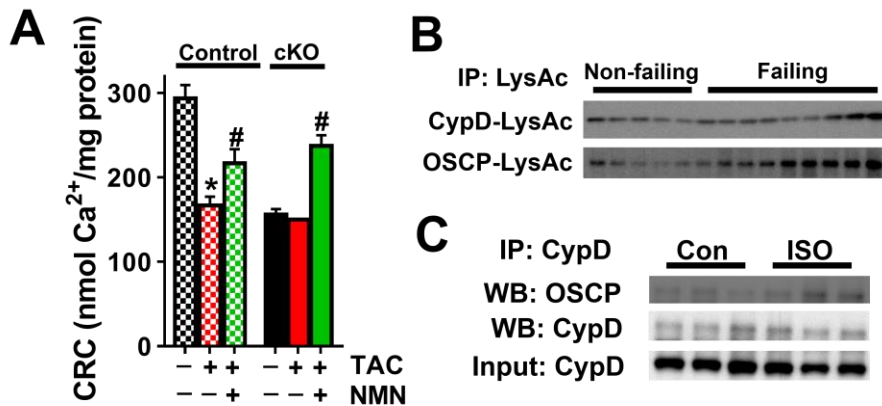


**Figure S6. Sensitivity of mPTP linked to OSCP and CypD acetylation. (A)** Calcium retention capacity (CRC) of isolated mitochondria as indicated was quantified. N=3-4. \*: P<0.05 compared to corresponding Sham; #: P<0.05 compared to corresponding TAC-VEH. **(B)** Acetylation of CypD and OSCP in normal and failing human hearts were determined by IP-WB. **(C)** Interaction of CypD and OSCP in hypertrophic hearts induced by ISO was determined by IP-WB. Data are expressed as means  $\pm$ SEM.



Figure S7, related to Fig. 7

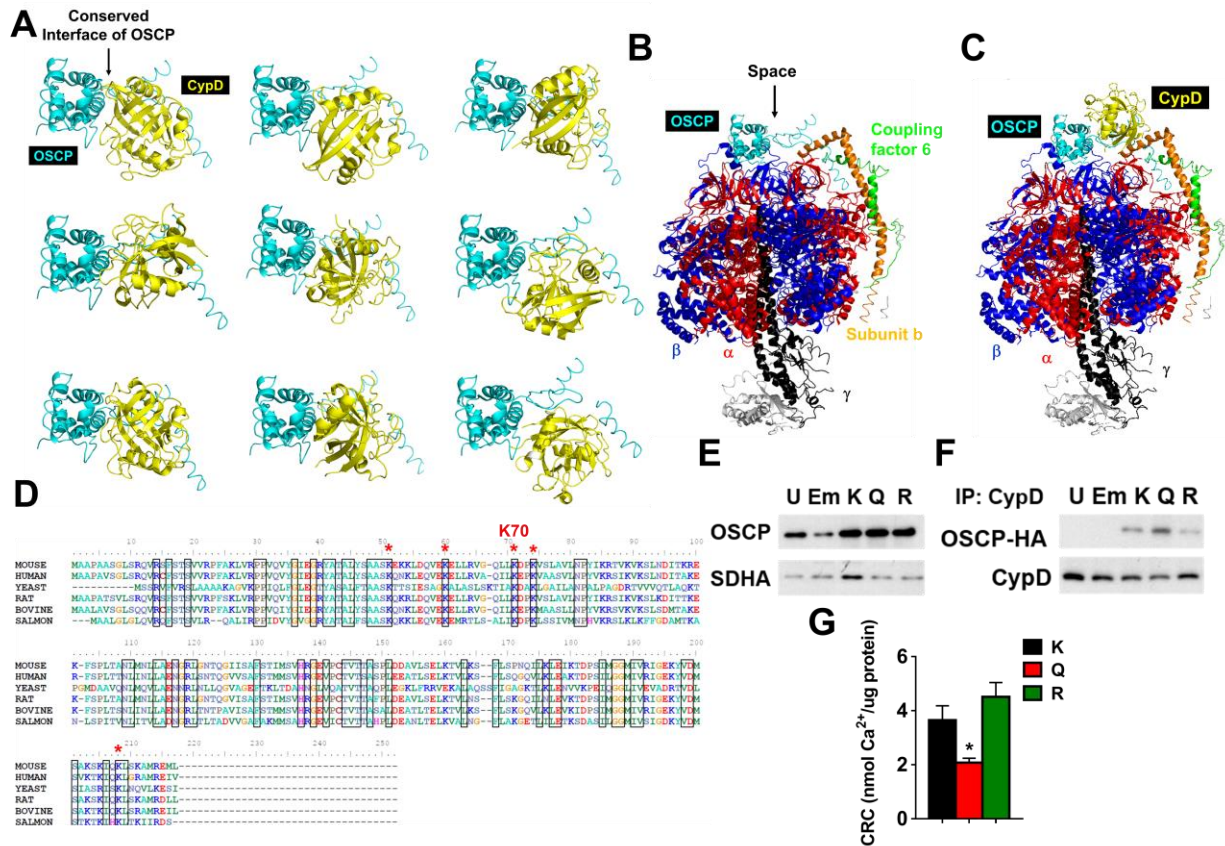


Figure S7. Structure-function relationship of OSCP-K70Ac with mPTP sensitivity.

(A) Nine highest scored docking solutions between OSCP (chain S only of 2WSS) and CypD (2BIU). OSCP protein orientations were similar in these solutions and in OSCP of panel B-C. (B) Picture depicting F<sub>1</sub>F<sub>0</sub>-ATP synthase complex (PDB: from 2WSS). A space is present allowing binding of CypD to the conserved interface of OSCP identified in (A). Alpha subunit: red. Beta subunit: blue. Gamma subunit: black. Coupling factor 6: green. Subunit b: orange. OSCP: cyan. (C) Picture showing one of the docking solutions of CypD with F<sub>1</sub>F<sub>0</sub>-ATP synthase complex. (D) Sequence alignment of OSCP proteins from mouse, human, yeast, rat, bovine and salmon shows OSCP-K70 is highly conserved among species (red asterisks) while other lysines may not. (E) Expression

levels and **(F)** interaction of OSCP-CypD of wild-type (K), K70Q (Q), and K70R (R) of OSCP variants in HEK293 cells were determined by Western blot. U: untransfected HEK293 cells. Em: empty pcDNA3.1 vector transfected cells. **(G)** CRC of permeabilized HEK293 cells treated as indicated were quantified. N=4-5. \*: P<0.05 corresponding to K. Data are expressed as means  $\pm$ SEM.

## **Supplementary table legends**

**Supplementary Table 1:** clinical data of the human subjects. ICM: ischemic cardiomyopathy. DCM: dilated cardiomyopathy. BMI: body mass index. EF: ejection fraction.

**Supplementary Table 2:** list of C-I proteins showed significant changes in levels from mitochondrial proteome analysis (cKO/Con > 2 or < 0.5; P<0.01, n=4).

**Supplementary Table 3:** list of cardiac mitochondrial proteins identified and spectral count values.

**Supplementary Table 4:** acetylated lysine sites of malate aspartate shuttle (MAS) proteins. K[170.11] depicts acetylation site. N/A: no peptide identified in Control but in cKO. N/D: not determined.

**Supplementary Table 5:** acetylated lysine sites of proteins linked to mPTP. K[170.11] depicts acetylation site. N/A: no peptide identified in Control but in cKO. N/D: not determined.

## **Supplementary methods**

### **Animal care, surgical procedures and echocardiography**

All procedures involving animal use were performed with the approval of IACUC of the University of Washington. Cardiac specific Ndufs4-KO mice (cKO) were generated as described <sup>1</sup>. Mice over-expressing NAMPT under the control of a-MHC promoter (cNAMPT) <sup>2</sup> were crossed with cKO to generate the desired genotypes as used in the experiments. Male mice (3-4 months old) underwent transverse aortic constriction (TAC) or sham surgery. Mice were anesthetized with sodium pentobarbital (75 mg/kg). Aorta

was exposed via a left thoracotomy and a constriction was made using a 7-0 ligature around the vessel and tied against a 27-gauge blunt needle. Sham surgeries were performed as above without performing the constriction of the aorta. NMN were delivered intraperitoneally to mice at 500 mg/kg once every three days 5-day before surgeries and 4-week after surgeries. Saline were delivered as control treatment. Echocardiography of hearts was performed at indicated time after surgery using the VEVO 770 system with a 707B scan head to lightly-anesthetized mice. Measurements were made when heart rate was within 500-600 bpm. Cardiac function and geometry measurements were measured in parasternal long axis B- and M-mode images and calculated by average of at least three cardiac cycles and carried out in a blind fashion. For experiments that mice were stressed by isoproterenol (30 mg/kg/day), isoproterenol was delivered by osmotic minipump (Alzet) for 2 weeks. Cardiac echocardiography was measured at baseline, 2-week and 4-week after implantation. Minipumps carrying saline were used as control. Hearts were harvested for mitochondrial isolated and subsequent biochemical assays.

### **Ex vivo measurements of cardiac function and energetics**

Langendorff perfused mouse hearts were isolated as previously described <sup>3, 4</sup> and maintained at a constant perfusion pressure of 80 mmHg at 37°C. Hearts were perfused with a buffer containing in mM; EDTA 0.5, KCl 5.3, MgSO<sub>4</sub> 1.2, NaCl 118, NaHCO<sub>3</sub> 25, CaCl<sub>2</sub> 2, mixed fatty acids 0.4 (bound to 1.2% albumin), Glucose 5.5, Lactate 1.2, and Insulin 50 mU/L. After an equilibration period of 30 minutes, hearts were switched to a buffer containing 4mM CaCl<sub>2</sub> to increase cardiac workload for 30 minutes. Left

ventricular function was monitored by a powerlab (AD Instruments) data acquisition system and high energy phosphate content was evaluated by  $^{31}\text{P}$  NMR spectroscopy.

### **Mitochondrial isolation, proteome, and acetylome analyses**

Mitochondria were isolated as described. For mitochondrial proteome analysis by mass spectrometry, 500ug of isolated mitochondria were resuspended in 0.2% SDS in ammonium bicarbonate buffer with protease inhibitor cocktail (Roche) and deacetylase inhibitors (nicotinamide, trichostatin A) and boiled for 5 minutes. The samples were reduced and alkylated with dithiothreitol (DTT) and iodoacetamide (IAA). Samples were diluted to 0.04% SDS and trypsinized with 10  $\mu\text{g}$  of sequencing grade trypsin (Promega) 37 °C overnight. Samples were loaded into MCX column (Waters) and washed by 0.1% and 0.01% trifluoroacetic acid (TFA). Samples were then eluted with 10%  $\text{NH}_4\text{OH}$ /90% methanol and dried for MS analysis.

For mass spectrometric analysis of mitochondrial proteome, peptide digestion products were analyzed by electrospray ionization on a linear ion trap Velos mass spectrometer (Thermo Scientific Corp., San Jose, CA). Nanoflow HPLC was performed using a Waters NanoAquity HPLC system (Waters Corporation, Milford, MA). Peptides were trapped on a 100  $\mu\text{m}$  i.d. x 20 mm long precolumn in-house packed with 200  $\text{\AA}$  (5  $\mu\text{m}$ ) Magic C18 particles (C18AQ; Michrom Bioresources Inc., Auburn, CA). Subsequent peptide separation was on an in-house constructed 75  $\mu\text{m}$  i.d. x 180 mm long analytical column pulled using a Sutter Instruments P-2000  $\text{CO}_2$  laser puller (Sutter Instrument Company, Novato, CA) and packed with 100  $\text{\AA}$  (5  $\mu\text{m}$ ) C18AQ particle. For each liquid

chromatography-tandem mass spectrometry (LC-MS/MS) analysis, an estimated amount of 1 µg of peptides (0.1 µg/µL) were loaded on the precolumn at 4 µL/min in water/acetonitrile (95/5) with 0.1% (v/v) formic acid. Peptides were eluted using an acetonitrile gradient flowing at 250 nL/min using mobile phase gradient of 5-35% acetonitrile over 500 min. with a total gradient time of 585 min. Ion source conditions were optimized using the tuning and calibration solution recommended by the instrument provider. Samples were analyzed in duplicates.

Acquired tandem mass spectra were searched for sequence matches against the IPI mouse database using SEQUEST. The following modifications were set as search parameters: peptide mass tolerance at 500 PPM, trypsin digestion cleavage after K or R (except when followed by P), one allowed missed cleavage site, carboxymethylated cysteines (static modification), and oxidized methionines or acetylation on K (variable modification). PeptideProphet <sup>5</sup> and ProteinProphet <sup>6</sup>, which compute the probability likelihood for each identification being correct, were used for statistical analysis of search results. PeptideProphet probability  $\geq 0.9$  and ProteinProphet probability  $\geq 0.9$  were used for positive identification at an error rate of less than 1%. Differences in relative expression of proteins were calculated using peptide spectral counting algorithm <sup>7</sup>.

For acetylome analysis, whole hearts of different genotypes were lysed with 0.2% SDS buffer with protease inhibitor cocktail (Roche) and deacetylase inhibitors (nicotinamide, trichostatin A). Lysis of heart tissue was aided by repeated freeze-thaw cycles and

homogenization. Soluble protein lysates were collected by centrifugation. Protein concentrations of lysates were measured by Lowry assay. 2mg of samples were reduced and alkylated with 5mM DTT and 10mM IAA. The samples were diluted to 0.04% SDS and digested by trypsin. The peptides were cleaned up by MCX cartridge (Waters), eluted with NH<sub>4</sub>OH/methanol buffer and dried for IP experiment. Dried samples were re-dissolved in IP buffer (50 mM MOPS pH 7.2, 10 mM NaPO<sub>4</sub>, 50 mM NaCl). Solubilized peptides were incubated with anti-acetyllysine antibody agarose (Immunechem) for 12 hours at 4 °C with gentle mixing. Agarose was washed with IP buffer and water. Acetylated peptides were eluted by 0.1% TFA in water and dried for MS analysis.

Enriched acetylation peptide samples were analyzed by LC-MS<sup>2</sup> using a Thermo Easy nLC coupled to a Q-Exactive Plus mass spectrometer. Peptide samples were loaded onto a trap column (3 cm x 100 µm i.d.) packed with 5 µm particle size, 200 Å pore size, Magic-C18AQ using a flow rate of 2 µl/min of solvent A (H<sub>2</sub>O containing 0.1% formic acid) for a total of 10 min. Peptides were then eluted from the trap column and separated by reversed-phase chromatography over a pulled tip, fused silica analytical column (60 cm 75 µm i.d.) packed with 5 µm particle size, 100 Å pore size, Magic-C18AQ, maintained at 45°C at a flow rate of 300 nL/min using a linear gradient from 90% solvent A/10% solvent B (acetonitrile containing 1% formic acid) to 70% solvent A/30% solvent B over 90 min followed by a 10 min wash with 20% solvent A/80% solvent B. Data dependent analysis (DDA) with the Q-Exactive Plus mass spectrometer consisted of a high resolution (70,000 RP) MS<sup>1</sup> scan followed by MS<sup>2</sup> (17,500) analysis

on the 20 most intense precursors. MS<sup>2</sup> settings included an AGC target value of 5x10<sup>4</sup>, a normalized collision energy of 25, isolation width of 1.6 *m/z*, activation time of 10 ms, activation Q of 0.25 and a minimum signal threshold of 10,000. Charge state exclusion was singly charged precursor ions, ions with charge state greater than six, and those with an undetermined charge state. Dynamic exclusion was enabled with an exclusion time of 30 s.

Comet (v2013.02 rev1) <sup>8</sup> was used to search the mass spectral data against the UniProt protein database for *Mus musculus* containing forward and reverse sequences (33224 total protein sequences). Comet search parameters included a precursor mass tolerance of 25 ppm, allowing for up to three <sup>13</sup>C offset. Trypsin was selected as the digesting enzyme allowing for up to two missed cleavage sites. Variable modifications included oxidation of Met (15.9949 Da) and acetylation on Lys or protein n-termini (42.010565 Da). Static modifications included carbamidomethylation of Cys (57.021464 Da). Fragment ion mass tolerance was set to 0.02 Da. Resulting peptide spectrum matches were filtered to <1% FDR using a forward/reverse sequence strategy.

Label free MS<sup>1</sup> based quantification of peptides was performed using MassChroQ <sup>9</sup>. Retention time alignment between LC-MS data files was performed using the obiwrap method. A 20 ppm tolerance was applied to generate extract ion chromatograms of precursor ions. Peak detection was accomplished using the zivy algorithm with a 30000 detection threshold on the max and a 15000 detection threshold on the min. The cKO/Control ratio of each acetylated peptide was estimated by the average value of four



hearts in each animal group. Standard error of the mean was calculated by the error propagation of standard deviation of the peptide in each animal group.

### **Molecular docking calculation**

Crystal structure data from PDB (2BIU and 2WSS, chain S) for CypD and OSCP proteins were subjected to rigid body molecular docking using online platform PATCHDOCK <http://bioinfo3d.cs.tau.ac.il/PatchDock/><sup>10</sup>. The ten highest scoring solutions without applying restriction to calculation were analyzed with the biomolecular visualization tool Pymol to highlight acetylated lysines on the OSCP and CypD complex. The putative interaction interface of OSCP (helix 1 and 5) was consistently observed from the ten solutions and is accessible for CypD binding into the 'space' in the intact F1-ATP synthase structure (Supplementary Fig. 5b,c). Another docking experiment was performed using all chains of 2WSS and 2BIU as input for docking with E36, K37, L40, R41, Q44, K47, L55, K77 on chain S of 2WSS (OSCP) defined as the interaction interface for CypD from the data of the first round docking. Acetylated lysines identified from proteomics analysis were mapped and specific acetylation of lysines at the interaction interface was determined as in Fig. 4f. Images were generated using Pymol.

### **Mitochondrial calcium uptake assay and biochemical assays**

In mitochondrial calcium uptake assay, 400 mg of mitochondria were incubated in 1-ml cuvette with mitochondrial assay buffer containing 10mM succinate, 120 mM KCl, 10 mM NaCl, 1 mM KH<sub>2</sub>PO<sub>4</sub> and 20 mM HEPES, 1.25 uM Fura FF (Molecular Probes) under constant stirring at 37 °C. 1 mM of CsA was added if indicated. Calcium uptake

was initiated with 25 nmol calcium pulse and measured spectrofluorometrically. Pulses were added at 2-minute interval until rapid calcium release (mPTP opening) occurred <sup>11</sup>. Calcium retention capacity was calculated as the amount of calcium needed to trigger mPTP opening. For permeabilized HEK293 cells <sup>12</sup>, the same setup and buffers were used. HEK293 cells were cultured without serum overnight and cells were lifted and washed with extracellular medium (20 mM HEPES, 120 mM NaCl, 5 mM KCl, 1mM KH<sub>2</sub>PO<sub>4</sub>, 0.2 mM MgCl<sub>2</sub>, 0.1 mM EGTA at pH 7.4). Cells were then permeabilized with digitonin (100 ug/ml) in mitochondrial assay buffer. The samples were pulsed with 5 nmol calcium.

NADH/NAD<sup>+</sup> levels were measured by assay kit (BioAssay). Malate aspartate shuttle capacities were measured as described <sup>13</sup>. Reaction buffer containing aspartate, ADP, NADH, malate dehydrogenase, glutamic oxaloacetate transaminase was mixed with 10 ug of mitochondria and the change at 340 nm were measured for 4 minutes at 37 °C as baseline oxidation of NADH. Substrate stock containing malate and glutamate were mixed with mitochondria and reaction buffer and the change at 340 nm were measured as malate/aspartate shuttle-driven oxidation of NADH. Lactate (Trinity Biotech), pyruvate (Abcam), acetyl-coA (Abcam) levels were measured with assay kits. In vitro acetylation of mitochondrial lysate by acetyl-coA was performed in 50 mM HEPES, 150 mM NaCl, pH 8.0 as described before <sup>14</sup>. Acetylated samples were analyzed by Western blot with acetyl-lysine antibody. Acetylated samples were immunoprecipitated by acetyl-lysine antibody agarose (Immunechem) and further analyzed with anti-GOT2 antibody (Santa Cruz). GOT activity were measured using commercially available kit (Sigma).

### **Antibodies, Western blot and immunoprecipitation**

Acetyl-lysine antibody (Cell Signaling), IDH3A (Abcam), PDHE1 (Abcam), OGDH (Abcam), CS, Uqcrc1, Uqcrb, Cox5b, GCN5L1, Sirt3 (Cell Signaling), VDAC1 (Santa Cruz), CypD (Abcam), OSCP (Abcam), Ndufs4 (Abcam), Ndufs3 (Abcam), Ndufb6 (Abcam), Ndufa9 (Abcam), SDHA (Abcam), ND1 (Abcam), ND2 (Abcam), ND3 (Abcam), ND4 (Abcam) and ND5 (Abcam). Cardiac tissues were homogenized with RIPA buffer (Sigma) using bullet blender at 4 °C for 10 minutes. Protein concentrations of supernatants were collected after centrifugation and quantified by Lowry assay. Protein lysates were loaded to 10 % SDS-PAGE, transferred to PVDF membrane and blocked with 5 % BSA in TSBT. Specific proteins were detected by specific antibodies listed above and corresponding secondary antibodies. Signals were visualized by HRP-derived chemiluminescence (Pierce) and film. Protein levels were quantified by Image-J. In acetylation analysis, cardiac mitochondria were lysed with RIPA buffer and further diluted by IP buffer (50 mM MOPS pH 7.2, 10 mM Sodium phosphate, 50 mM Sodium chloride). IP buffer pre-washed acetyl-lysine antibody-conjugated agarose (Immunechem, Burnaby) was incubated with the cleared lysate at 4 °C overnight with mild agitation. Agarose bound with acetylated proteins was washed gently with IP buffer for three times by centrifugation. Bound acetylated proteins were released by SDS loading buffer and 5-minute heating at 95 °C. Samples were loaded to SDS-PAGE for analysis.

In co-immunoprecipitation of CypD or OSCP, isolated mitochondria were lysed with buffer containing detergent digitonin. Lysate were mixed with CypD (Abcam) antibodies. Antibodies bound proteins were precipitated with IgA/G agarose (Santa Cruz) and washed three times with lysis buffer. Samples were prepared with SDS-PAGE buffer and boiled for further analysis by Western blotting.

### **Statistical analysis**

Comparisons among the multiple groups were performed by 1-way ANOVA, followed by Newman-Keuls multiple comparison test. For comparisons only involving two groups, unpaired 2-tailed t-tests were used. For repeated measurements of multiple groups, 2-way repeated measure ANOVA was performed. All analyses were performed using GraphPad Prism 6.0. All data are expressed as mean  $\pm$  SEM and a  $p < 0.05$  was considered significant.

### **References**

1. Karamanlidis G, Lee CF, Garcia-Menendez L, Kolwicz SC, Jr., Suthammarak W, Gong G, Sedensky MM, Morgan PG, Wang W and Tian R. Mitochondrial complex I deficiency increases protein acetylation and accelerates heart failure. *Cell Metab.* 2013;18:239-50.
2. Hsu CP, Oka S, Shao D, Hariharan N and Sadoshima J. Nicotinamide phosphoribosyltransferase regulates cell survival through NAD<sup>+</sup> synthesis in cardiac myocytes. *Circ Res.* 2009;105:481-91.
3. Yan J, Young ME, Cui L, Lopaschuk GD, Liao R and Tian R. Increased glucose uptake and oxidation in mouse hearts prevent high fatty acid oxidation but cause cardiac dysfunction in diet-induced obesity. *Circulation.* 2009;119:2818-28.

4. Kolwicz SC, Olson DP, Marney LC, Garcia-Menendez L, Synovec RE and Tian R. Cardiac-Specific Deletion of Acetyl CoA Carboxylase 2 (ACC2) Prevents Metabolic Remodeling During Pressure-Overload Hypertrophy. *Circ Res*. 2012.
5. Keller A, Nesvizhskii AI, Kolker E and Aebersold R. Empirical statistical model to estimate the accuracy of peptide identifications made by MS/MS and database search. *Anal Chem*. 2002;74:5383-92.
6. Nesvizhskii AI, Keller A, Kolker E and Aebersold R. A statistical model for identifying proteins by tandem mass spectrometry. *Anal Chem*. 2003;75:4646-58.
7. Liu H, Sadygov RG and Yates JR, 3rd. A model for random sampling and estimation of relative protein abundance in shotgun proteomics. *Anal Chem*. 2004;76:4193-201.
8. Eng JK, Jahan TA and Hoopmann MR. Comet: an open-source MS/MS sequence database search tool. *Proteomics*. 2013;13:22-4.
9. Valot B, Langella O, Nano E and Zivy M. MassChroQ: a versatile tool for mass spectrometry quantification. *Proteomics*. 2011;11:3572-7.
10. Schneidman-Duhovny D, Inbar Y, Nussinov R and Wolfson HJ. PatchDock and SymmDock: servers for rigid and symmetric docking. *Nucleic Acids Res*. 2005;33:W363-7.
11. Marcu R, Neeley CK, Karamanlidis G and Hawkins BJ. Multi-parameter measurement of the permeability transition pore opening in isolated mouse heart mitochondria. *J Vis Exp*. 2012.
12. Wiczer BM, Marcu R and Hawkins BJ. KB-R7943, a plasma membrane Na(+)/Ca(2+) exchanger inhibitor, blocks opening of the mitochondrial permeability transition pore. *Biochem Biophys Res Commun*. 2014;444:44-9.
13. Scholz TD and Koppenhafer SL. Reducing equivalent shuttles in developing porcine myocardium: enhanced capacity in the newborn heart. *Pediatr Res*. 1995;38:221-7.
14. Wagner GR and Payne RM. Widespread and enzyme-independent Nepsilon-acetylation and Nepsilon-succinylation of proteins in the chemical conditions of the mitochondrial matrix. *J Biol Chem*. 2013;288:29036-45.